Chapter -5

Full Energy Peak Efficiency Calibration of HPGe detector by MCNP

5.1 Introduction

As emphasized in Chapter 2, calculation or measurement of full energy peak (*FEP*) efficiency for particular source-detector geometry is essential for quantitative analysis of any radionuclide by gamma ray spectrometry. Efficiencies at a particular gamma ray energy *E* is experimentally obtained by using a gamma ray source (emitting photon of energy *E*) of known disintegration rate. The calibration of FEP efficiency as a function of gamma ray energy is known as FEP efficiency calibration of a gamma ray detector. Since no two detectors can have exactly the same sensitive volume, there efficiencies can never exactly match so that each gamma ray detector has to be individually calibrated for its efficiency to get reliable results.

5.2 Efficiency calibration: *Different methods*

For routine gamma spectrometric analysis, efficiency calibration of a gamma ray detector is carried out using a set of standards emitting gamma rays over the energy range of 50-1500 keV. Full energy peak efficiency calibration is preferably done using the monoenergetic gamma ray sources e.g. ^{241}Am, ^{109}Cd, ^{57}Co, ^{139}Ce, ^{203}Hg, ^{51}Cr, ^{113}Sn, ^{85}Sr, ^{137}Cs and ^{65}Zn. The gamma ray energies and abundances along with the half-lives of these radionuclides are given in Table 5.1. However, the availability of monoenergetic primary standards is a constraint. Moreover, some of these sources are not very long lived e.g. ^{203}Hg ($t_{1/2}$-46.6 d), ^{51}Cr ($t_{1/2}$-27.7 d), so they need to be replaced periodically.

Table 5.1 Monoenergetic sources used as calibration sources.

Nuclide	Energy (keV)	Gamma ray Abundances (%)	Half-life
^{109}Cd	88.04	3.6	462.2 d
^{57}Co	122.06	85.6	271.8 d
^{139}Ce	165.86	79.9	137.6 d
^{203}Hg	279.2	81.5	46.6 d
^{51}Cr	320.1	98.6	27.7 d
^{113}Sn	391.7	64.0	115.1 d
^{85}Sr	514.0	95.7	64.9 d
^{137}Cs	661.6	85.1	30.2 y
^{65}Zn	1115	50.6	244.3 d

Multi-gamma ray sources like ^{152}Eu (13.5 y), ^{133}Ba (10.5 y), ^{110}Ag^{m} (249.9 d), ^{226}Ra (1.6 x 10^{3} y) and ^{56}Co (78.8 d) are often preferred for efficiency calibration as they cover a wide energy range and are longer lived. The gamma ray energies of these radionuclides are given in Table 5.2. However, these sources emit gamma rays in cascade and for close sample-to-detector distances, there may be substantial coincidence summing leading to inaccuracy in efficiency calibration. Therefore, standard multi-gamma sources cannot be used for efficiency calibration of a detector at close sample-to-detector distance. However, gamma spectrometric analysis of low level samples needs to count the samples

as close as possible to the detector. These difficulties can be circumvented using Monte Carlo simulation for full energy peak efficiency.

Table 5.2 Multi-energetic sources used as calibration sources.

Nuclide	Energy (keV)	Gamma ray abundance (%)	Nuclide	Energy (keV)	Gamma ray abundance (%)
^{152}Eu	121.78	28.4	^{133}Ba	81	34.1
	244.69	7.5		160.6	64.5
	344.28	26.6		276.4	7.16
	444.0	2.8		302.9	18.33
	778.9	13.0		356	62.05
	964.05	14.6		383.9	8.84
	1112.0	13.5	^{56}Co	846.8	99.9
	1408.03	20.8		1037.8	14.0
^{110}Ag^{m}	657.7	94.0		1238.3	67.6
	677.6	10.3		1771.4	15.7
	706.7	16.3		2598.6	17.3
	763.9	22.1	^{226}Ra	295.2	18.5
	884.7	75.9		351.9	35.8
	937.5	34.1		609.3	44.8
	1384.3	24.1		1120.3	14.8
	1505.0	12.9		1764.5	15.4

5.3 Monte Carlo Method

It is a powerful tool to simulate the detector response and is applicable to a variety of sample matrices and geometries [Sima and Arnold (2009), Vidmar et al. (2008), Tzika et al. (2004), Ródenas et al. (2003), Ewa et al. (2001)]. The basic principle of this method has been discussed in Chapter 1. Monte Carlo methods were first used by Wainio and Knoll (1966) and De Castro Faria and Levesque (1967) for full energy peak efficiencies calculations. Bronson and Wang (1996) have given an extensive description on the use of the Monte Carlo method for efficiency determination at various source–detector geometries (on and off detector axis), complex source shapes and Marinelli beaker models. General Monte Carlo codes like MCNP [Wang et al. (1994), Kamboj and Kahn (1996), Fehrenbacher et al. (1996), Glouvas et al. (1998), Rodenas et al. (2000)], GEANT [Glouvas et al. (1998), Sanchez et al. (1991), Decombaz et al. (1992), Garcia-Talavera (2000), Korun et al. (1997)], EGS4 [Fehrenbacher et al. (1996)], CYLTRAN [Ludington and Helmer (2000)] are also being tested extensively. These codes are increasingly used to simulate efficiency for cases where experimental determination is impossible or difficult such as samples of nonstandard geometry and for large sized samples e.g. environmental samples [Nakamura and Suzuki (1983)] and waste drums where standards are not easily available. Also, these simulation methods are decay scheme independent and are consequently free of any coincidence summing. Therefore, these methods can be used to obtain FEP efficiency at closest sample-to-detector distance where multi-gamma ray sources cannot be used. Additionally, these simulation codes can be used to get total efficiency required for coincidence summing correction. However, as reported in most of the literature, there is often a mismatch between the simulated and experimental

efficiencies. This is due to the inaccuracy of the detector geometry specifications given by the manufacturer. The dimensions provided by the manufacturer correspond to the time of assembly of the detection system at room temperature. But there can be changes in the mechanical support of the crystal due to contractions at low temperature leading to changes in the detector configuration [Johnston et al. (2006)]. Also, there can be uncertainty in the parameters e.g. dead layer thickness, detector end cap to Ge crystal distance etc. The problem can be overcome by either determining the dimensions of detector or by adjusting the detector parameters such that the simulated efficiencies match with the experimental efficiencies. The studies in literature available for both the methods have been discussed in the subsequent sections.

5.3.1 Detector Parameters Determination

Crystal parameters and position

There are reports in literature in which the physical characteristics of the detector have been measured experimentally to minimize these uncertainties [Helmer et al. (2003), Hardy et al. (2002), Dryak and Kovar (2006), Budja´sˇ et al. (2009)]. The shape, dimensions and location of the crystal have been found out using gamma or X-ray radiography [Dryak and Kovar (2006), Budja´sˇ et al. (2009), Johnston (1985), Boson (2008)]. Typical X-ray and gamma ray radiographs have been shown in Figure 5.1. A number of photographs from different directions are needed to get the detector position and its displacement from the crystal axis. The length of the sensitive region of the detector has also been determined by scanning the detector along its axis and accuracy less than 1% has been achieved between experimental and calculated efficiency [Helmer

et al. (2003), Hardy et al. (2002), Debertin and Grosswendt (1982)]. The energy of the gamma ray photon used for scanning is chosen in such a way that it should be high enough to penetrate the window and detector housing and it should be low enough to be sensitive to the thickness of any attenuating layers and is effectively collimated by the collimator. Debertin and Grosswendt (1982) used a collimated beam of gamma ray from ^{241}Am source with a 20 mm long lead collimator with a 1 mm hole in diameter. The source-collimator assembly was moved in 1 mm steps and the counts at 59.5 keV peak were monitored. Several scans, along different diameters or along lines parallel to one another, were carried and the position, diameter, and thickness of the sensitive volume could thus be determined with a resolution of 1 mm. The diameter of the insensitive core of the true co-axial detector has also been measured in this way.

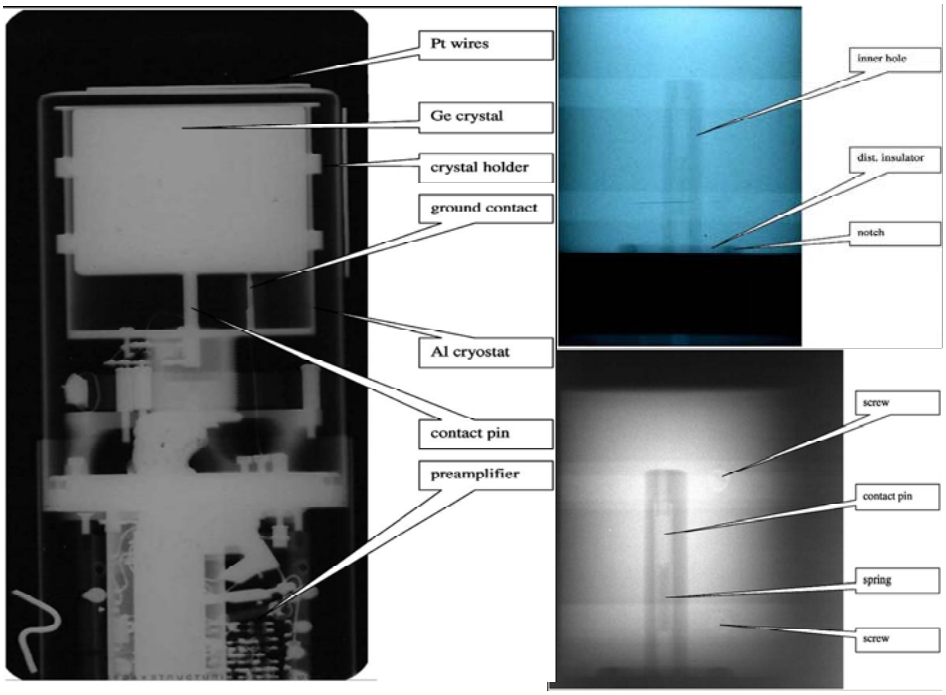

Figure 5.1 X-ray and gamma ray radiographs of an HPGe detector [Dryak and Kovar (2006)].

Windows and dead layers

The photons before reaching the detector have to pass through the detector window and dead layer in front of the crystal and are subjected to attenuation in these materials depending upon their *Z*. This absorption or scattering of the gamma ray in these materials are the ones responsible for the peaked nature of the efficiency curve. This is because although the interaction probability of a gamma ray decreases with increasing gamma ray energy but the lower energy gamma rays are absorbed in the detector window and dead layers, due to which the probability of low energy gamma rays reaching the crystal decreases. Due to this, as gamma ray energy increases, the efficiencies first increases, reaches a maximum and then decreases. The dead layer thickness specified by the manufacturer is frequently inaccurate. Also, it has been observed that there can be increase in dead layer thickness from 0.35 mm to 1.16 mm after 9 years of operating time [Huy et al. (2007)]. The inhomogeneity in the dead layer thickness has also been shown by Debertin and Grosswendt (1982) and Keyser (2004). The average dead layer thickness is generally measured by measuring the attenuation of a collimated photon beam. The average dead layer thickness on front face and on the cylindrical side of the crystal has been measured by using ^{241}Am source [Budja´sˇ et al. (2009)]. Another method [Forcinal (1973), Pessara (1983)] to measure the thickness of a material takes advantage of the abrupt change in the mass attenuation coefficient near the K-edge of the material. The ratio of the peak counts of photons just above the K-edge and just below the K-edge is used to calculate the thickness of the dead layer, assuming that the change in efficiency in such a small energy range is negligible. This method has been used to determine the thickness of Ge dead layer. The mass attenuation coefficient of Ge changes from μ/ρ =

27 cm^2g^{-1} below the K-edge at 11.1 keV to 209 cm^2g^{-1} above it. ^{75}Se source is used as it emits As X-rays with the K_α lines at 10.5 keV slightly below and the K_β lines at 11.7 keV slightly above the Ge K-edge and the thickness can be obtained from the equation:

$$N_\alpha / N_\beta = 6.55e^{0.073t} \tag{5.1}$$

where N_α and N_β are the counts in the K_α and K_β peaks and t is the thickness of Ge dead layer in μm. Baker et al. (1987) determined the Be-window and Si-dead layer thickness by making measurements at several energies, above and below the Si K-edge, with well-collimated X-ray beams, incident normal to the detector surface and at an angle of 38.5° to the normal. Another method available in literature for measuring gold contact and silicon dead layer of a Si(Li) detector is by exciting the gold and silicon dead layer atoms with photons of energy greater than the gold L- and silicon K-absorption edges and measuring the characteristic Au L, and Si K X-rays [Maenhaut & Raemdonck (1984), Shima (1980)]. Another method for determining the thicknesses of different absorbing layers including end-cap thickness is based on positioning the source collimator at two places such that photon beam could hit the detector surface at two different angles of incidence relative to the crystal surface, 45° and 90° [Dryak and Kovar (2006), Van Riper et al. (2002), Boson (2008)]. The thickness of the absorbing layers can then be calculated from the relative change in the count rate between the two angles. Nir-El and Sima (2001) have also used ultrasound probe measurements to verify the thickness of the end cap.

5.3.2 Effect of Detector Parameters on the FEP Efficiency

The effect of different detector parameters on the FEP efficiency has been studied in literature [Vargas et al. (2002), Kamboj and Kahn (2003)]. Vargas et al. (2002) varied detector parameters such as crystal diameter, crystal length, diameter of the internal core, and the position of the crystal with respect to the Be window and observed that the efficiency varies significantly with the crystal diameter and its position. It has been observed that it is the detector overall volume and not the detector diameter or length that has a major effect on the FEP efficiency [Kamboj and Kahn (2003)]. Bochud et al. (2006) observed that along with the crystal diameter and length, it is the dead layer in front of the detector surface which affects largely the detector's efficiency. The influence of dead layer thickness on the detector efficiency response has also been studied [Ródenas et al. (2003)]. They observed that increase of dead layer thickness leads to the decrease in the detector's efficiency, not only due to attenuation of gamma rays in the dead layer but also due to the reduction of the active volume of the detector.

5.3.3 Optimization of Detector Geometry

Due to the uncertainty in the detector parameters, which may result in uncertainty in efficiency calculation by Monte Carlo method, a general approach has evolved whereby the different detector parameters are optimized to reproduce the experimental point source efficiencies as a function of energy. Subsequently, efficiency for other geometries can be obtained accurately using the optimized detector parameters. Crystal dimensions such as the crystal diameter, length and crystal front dead layer thickness has been adjusted and results have been obtained with a relative deviation of 5-10% [Liye et al.

(2004), Binquan et al. (2005), Bochud et al. (2006)]. Tzika et al. (2010) optimized the detector geometry by changing the dead layer thickness and could get an overall agreement of 10%. Karamanis (2003) also increased Ge-Al end cap distance by 8 mm and the entrance Li dead layer by 600 μm to get results within 5%. In EUROMET exercise [Lepy et al. (2001)], it was concluded that most of the simulation codes can be used for routine measurements where uncertainties of 5-10% in efficiencies are acceptable. There is literature where much better accuracy (< 2%) has been obtained by optimizing the detector geometry [Helmer et al. (2003), Hardy et al. (2002), Wang et al. (2002)]. Budjas et al. (2009) could obtain an accuracy of ~ 3% by adjusting the dead layer thickness and inner hole radius of a p-type detector.

5.4 Objective of the Work

The aim of this work was to optimize the HPGe detector parameters that is routinely used in our lab for gamma spectrometric measurements. This was done by using experimental efficiencies for standard geometries such as point sources. The optimized detector parameters have been used for efficiency transfer to other geometries. Results are discussed in the light of existing observations in the literature.

5.4.1 Gamma Spectrometric Measurements

The detector used in the present work was a closed end co-axial p-type DSG HPGe detector. The detector had a 20% relative efficiency and a resolution of 2.1 keV for the ^{60}Co gamma ray at 1332 keV. The schematic diagram of the detector geometry as specified by the manufacturer is shown in Figure 5.2.

The detector was first calibrated for its efficiency by counting point sources of standard ^{133}Ba and ^{152}Eu at 21.7 cm from the detector end cap. Such a large distance was chosen for efficiency calibration with these multi-gamma sources so as to avoid any uncertainty in the efficiency curve due to coincidence summing. The counting of the samples was done for a sufficiently long time so as to keep statistical uncertainty less than a percent.

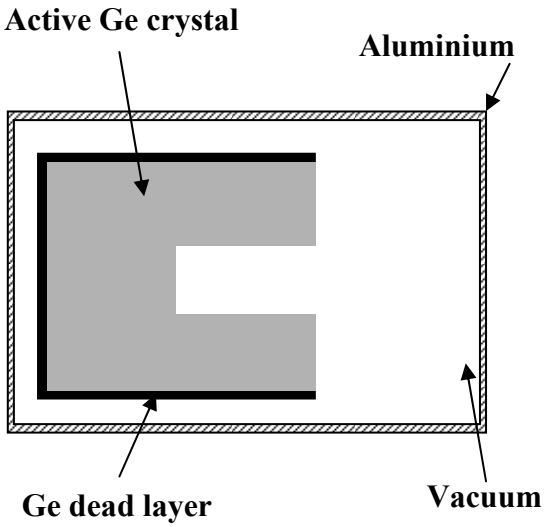

Figure 5.2 Schematic diagram of the detector geometry supplied by the manufacturer.

All the spectra were analyzed by PHAST software [Mukhopadhya (2001)], the detail of which is given in Chapter 2. The Eu-Ba efficiencies were fitted into a fourth order log-log polynomial curve by non-linear least square fitting. These efficiencies were then used to obtain dps of point sources of ^{109}Cd, ^{57}Co, ^{203}Hg, ^{51}Cr, ^{137}Cs and ^{65}Zn prepared from the activities procured from Board of Radiation and Isotope Technology, Mumbai. For this, these sources were also counted at d = 21.7 cm. The monoenergetic sources were then used to determine FEP efficiencies (ε_γ) at closer distances (d = 1.7 and 12.6 cm) by using the experimentally determined disintegration rate (*dps*) given by:

$$\varepsilon_\gamma = \frac{cps}{I_\gamma x\, dps} \tag{5.2}$$

where *cps* is the count rate at the energy of interest and I_γ is the gamma ray emission probability taken from Table of Isotopes [Firestone (1996)]. The count rates were corrected for the background peak counts in all the cases.

Similarly, 5 ml sources of ^{109}Cd, ^{57}Co, ^{203}Hg, ^{137}Cs and ^{65}Zn were calibrated using standard 5 ml sources of ^{152}Eu and ^{133}Ba in same HPGe detector at d = 10.3 cm. Such a large distance was chosen so that the coincidence summing effects are negligible. These sources were then used to obtain efficiencies at d = 2.0 cm. Also, 100 ml standard source of ^{152}Eu taken in a glass bottle was counted in the same HPGe detector at d = 19.8 cm and FEP efficiencies were determined.

5.4.2 Monte Carlo Simulation

In this work, the version MCNP4c [Briesmeister (2000)] was used to simulate the HPGe detector response. This code tracks the particle from its origin to the point of its complete absorption. All primary as well as secondary interactions are taken into account. The efficiency was obtained with *F8* tally which is a pulse height tally without any variance reduction. Mode *P* was used. The description of the detector geometry was given in detail in the cell and surface cards of the MCNP input file. The detector housing including the absorbing materials (aluminum end cap, germanium dead layer), were all included in the geometry. In each run ~10^8 particles were sampled to reduce statistical uncertainties.

5.4.3 Comparison of MCNP and Experimental Efficiencies

Initial MCNP simulations were performed for point source geometry with the dimensions of the detector obtained from manufacturer as given in the second column of Table 5.3. The MCNP simulated and experimental values of the FEP efficiencies are shown in Figure 5.3. The error on experimental efficiencies is also shown in the figure and is obtained by propagating the error on peak areas, abundances and efficiency fitting error. The error bars are of the size of the symbol.

Table 5.3 Detector parameters provided by manufacturer and optimized by MCNP simulation.

Description	Manufacturer supplied value (mm)	Optimized value (mm)
Crystal radius	24.55	23.65
Crystal length	49.9	49.9
Front Ge dead layer thickness	0.6	0.7
Side Ge dead layer thickness	0.6	0.6
Inner hole radius	4.25	4.25
Inner hole depth	38.4	38.4
Al end cap thickness	0.7	0.7
Al end cap to crystal distance	3	9

At all sample-to-detector distances (d = 1.7 cm, 12.6 cm and 21.7 cm), the MCNP efficiencies were found to be higher than the experimental values indicating the inadequacy of the manufacturer supplied detector dimensions. Similar observations have

also been made in literature [Helmer et al. (2003), Budja´sˇ et al (2009), Vargas et al. (2002), Laborie et al. (2000)]. A more detailed comparison of the MCNP and experimental efficiencies at d = 1.7 cm, 12.6 cm and 21.7 cm has been given in Table 5.4. At a particular distance, the ratios of MCNP to experimental efficiencies were observed to be constant within 2-4% over the energy range of 88-1115 keV. But, these ratios were found to vary strongly from one distance to other with the MCNP to experimental ratio being higher at closer distance. It can be seen from the table that the average MCNP to experimental ratio at d = 21.7 cm is 1.14 while it increases to 1.20 at d = 12.6 cm and to 1.46 at d = 1.7 cm. This indicates that the detector parameters have to be adjusted such that the constancy of ratio of efficiency over the energy range is not disturbed but the strong dependency on the sample-to-detector distance is removed.

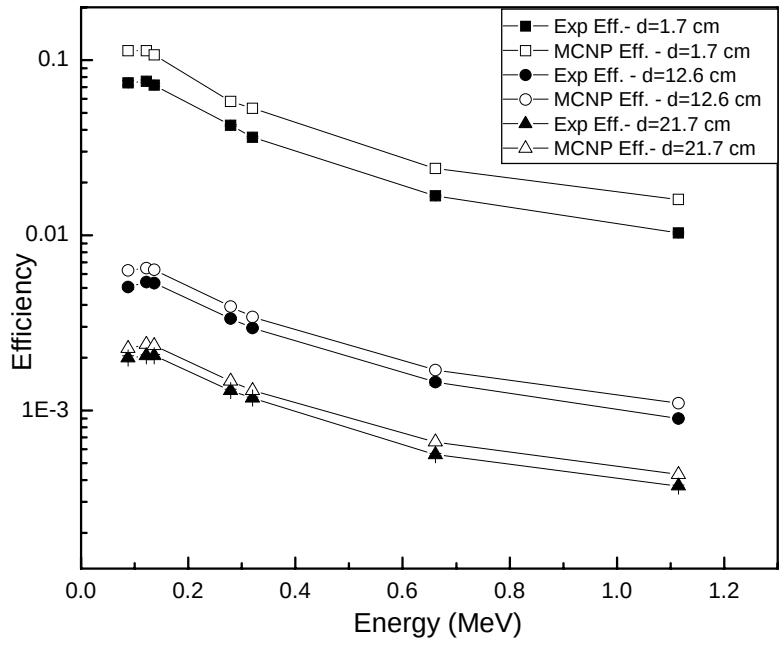

Figure 5.3 Experimental and MCNP simulated FEP efficiency for point source geometry using the manufacturer supplied detector geometry at three sample-to-detector distances, d = 1.7 cm, 12.6 cm and 21.7 cm.

5.5. Optimization of different detector parameters

There are a number of geometrical parameters which can be uncertain like detector crystal radius, its length, inner hole radius and length, dead layer thickness, Al end cap thickness, the Al end cap to detector crystal distance. The effect of systematic change in these parameters on the FEP efficiency is discussed in the following.

Table 5.4 The comparison of experimental and MCNP efficiencies at three sample-to-detector distances, *d* = 1.7 cm, 12.6 cm and 21.7 cm. The detector geometry used has been provided by the manufacturer.

Energy	**d = 1.7 cm**			**d = 12.6 cm**			**d = 21.7 cm**		
(MeV)	**MCNP eff**	**Exp eff**	**MCNP /Exp**	**MCNP eff**	**Exp eff**	**MCNP /Exp**	**MCNP eff**	**Exp eff**	**MCNP /Exp**
0.088	0.1132	0.0741	1.53	0.0063	0.0051	1.24	0.0023	0.0020	1.14
0.122	0.1126	0.0757	1.49	0.0065	0.0054	1.20	0.0024	0.0020	1.16
0.136	0.1073	0.0720	1.49	0.0064	0.0053	1.19	0.0023	0.0020	1.14
0.279	0.0579	0.0424	1.36	0.0039	0.0033	1.17	0.0015	0.0013	1.13
0.320	0.0525	0.0363	1.44	0.0034	0.0030	1.16	0.0013	0.0012	1.11
0.661	0.0238	0.0168	1.41	0.0017	0.0015	1.17	0.0007	0.0006	1.17
1.115	0.0155	0.0103	1.50	0.0011	0.0009	1.22	0.0004	0.0004	1.15
		Avg.	1.46		**Avg.**	1.20		**Avg.**	1.14
		Std. Dev.	0.06		**Std. Dev.**	0.03		**Std. Dev.**	0.02
		% RSD	3.92		**% RSD**	2.52		**% RSD**	1.90

5.5.1 Detector Crystal Geometry

Since crystal dimensions have been reported to have major effect on the detector efficiency, the radius of the detector was reduced by 1 mm and detector efficiency was computed by MCNP at d = 1.7 and 21.7 cm. Table 5.5 gives the comparison of FEP experimental and MCNP efficiency results. The average efficiency ratio has reduced from 1.46 to 1.36 at 1.7 cm and from 1.14 to 1.03 at d = 21.7 cm. The detector radius was further reduced by 1 mm, to see if the ratio further reduces and approaches unity. As given in Table 5.5, although at d = 1.7 cm, the ratio has reduced to 1.16 but it became less than 1 at d = 21.7 cm. Thus, it can be concluded that the reduction in crystal radius by 1 mm can reproduce the experimental efficiency at long distance, but at shorter distance (d = 1.7 cm), the discrepancy still exists. Since the MCNP to experimental ratio should be close to unity at all sample-to-detector distance, variation of crystal radius alone is not sufficient to match MCNP and experimental efficiency.

Since the crystal length can also have appreciable effect on efficiency, as a next step, it was reduced by 4.9 mm keeping the inner hole length constant, and as given in Table 5.5, the average MCNP to experimental ratio at both the distances decreased by about 2-3% only even after a reduction of detector length by 10%. Since the value of length quoted by the manufacturer could not be erroneous by more than 10%, this parameter was not further changed and its original value was restored. The increment in inner hole radius to 5.75 mm and thereby reduction in the overall detector volume, as given in Table 5.5, introduced energy dependence which was earlier not present with the manufacturer supplied detector geometry. This was expected as the lower energy gamma rays will be absorbed in a small detector length and so will not be affected by increasing the inner

hole radius but some part of the high energy gamma rays will escape due to increase in the inner hole radius. Therefore, in the present case, this was not the parameter to be changed.

Table 5.5 The ratio of MCNP and experimental efficiencies at two sample-to-detector distances, d = 1.7 cm and 21.7 cm. The MCNP efficiencies are computed by changing some detector crystal parameters to see its effect on the detector efficiency.

Energy (MeV)	**Crystal radius reduced by 1 mm**	**Crystal radius reduced by 2 mm**	**Crystal length reduced by 4.9 mm**	**Inner hole radius increased by 5.75 mm**	**Dead layer thickness increased by 0.4 mm**
	FEP efficiencies (MCNP/Exp)				
	d = 1.7 cm				
0.088	1.46	1.31	1.53	1.53	1.29
0.122	1.41	1.25	1.49	1.44	1.37
0.136	1.41	1.24	1.49	1.40	1.40
0.279	1.27	1.08	1.35	0.95	1.33
0.320	1.34	1.13	1.42	1.33	1.41
0.661	1.29	1.05	1.36	1.22	1.39
1.115	1.36	1.09	1.43	1.26	1.48
Avg.	1.36	1.16	1.44	1.31	1.38
Std. Dev.	0.07	0.10	0.07	0.19	0.06
% RSD	5.04	8.58	4.69	14.36	4.37
	d = 21.7 cm				
0.088	1.05	0.88	1.14	1.13	0.99
0.122	1.07	0.89	1.16	1.14	1.09
0.136	1.04	0.88	1.13	1.11	1.08
0.279	1.03	0.84	1.10	1.02	1.11
0.320	1.00	0.81	1.07	0.97	1.08
0.661	1.06	0.83	1.11	0.97	1.17
1.115	1.02	0.79	1.06	0.91	1.13
Avg.	1.04	0.85	1.11	1.04	1.09
Std. Dev.	0.02	0.04	0.04	0.09	0.06
% RSD	2.26	4.48	3.22	8.72	5.06

The detector efficiency also depends upon the dead layer thickness, as low energy photons may be highly attenuated in it. The influence of dead layer thickness on the detector efficiency was seen by increasing the dead layer thickness by 0.4 mm. There was a reduction of only 4-5% in the MCNP to experimental efficiency ratios as given in Table 5.5 after an increase in dead layer thickness by 67%. From this, it was concluded that, in our case the detector crystal parameters are not the one responsible for such a high efficiency ratio of 1.46 at d = 1.7 cm.

5.5.2 Detector End Cap Thickness and End Cap to Crystal Distance

Since the effect of increasing the thickness of Al end cap will be similar and less in magnitude to increasing the Ge dead layer thickness, the Al thickness was not changed. The distance between the Al end cap and detector crystal (d_{alc}) was increased by 3 mm and MCNP efficiencies were computed at d = 1.7 and 21.7 cm. Table 5.6 gives the MCNP and experimental efficiency values and their ratios. The MCNP efficiencies at 1.7 cm decreased by about 13% while the efficiencies at d = 21.7 cm reduced by only 2%. Since in our case, there is distance dependence in the MCNP to experimental ratio with the ratio being higher at closer distance, the Al end cap to crystal distance was identified as the main cause of discrepancy between MCNP and experimental efficiency values. This is in accordance with Hardy et al. (2002) who observed an uncertainty of ~36% in the Al end cap to crystal distance. The d_{alc} was then systematically changed and the results are presented in Table 5.6. When the Al end cap to crystal distance is kept as 8 mm, the ratio of efficiencies was further decreased, but still a difference between the efficiency ratios at d = 1.7 cm and 21.7 cm could be seen. The principle of efficiency

transfer says that this difference should not exist, the Al end cap to crystal distance was further incremented in steps to 1 mm. The results are given in Table 5.6. It could be seen that as the Al end cap to crystal distance was increased, the ratios of MCNP to experimental efficiencies at d = 1.7 cm and 21.7 cm came closer and almost coincided at Al end cap to crystal distance of 9 mm and after that again diverged. This indicates that the Al end cap to crystal distance should be taken as 9 mm instead of 3 mm (quoted by the manufacturer) to get a MCNP to experimental efficiency ratio independent of sample-to-detector distance.

Experimental validation

To experimentally verify the deviation in Al end cap to crystal distance from the manufacturer supplied value, the detector was axially scanned. For this a ^{109}Cd source was used and its count rate was measured through a 3 mm collimator in touching configuration with detector. Figure 5.4 gives the axial profile from the surface of the detector. It can be seen that the count rate is minimum at 3 mm from the detector surface and increases only after 5 mm and becomes maximum at 15 mm so that the average distance of Al end cap to crystal distance can be roughly considered as 10 mm. However a better estimate is expected if the collimator diameter is reduced to 1 mm.

But, the MCNP efficiencies were still found to be 10% higher than the experimental values at both the sample-to-detector distances. Further optimization was carried out to bring this factor close to unity. Previously, from Table 5.5, it was observed that when the detector radius is reduced by 1 mm, the efficiency ratio also reduces by about 7-9% at the two sample-to-detector distances. This will bring the efficiency ratio close to 1 if the

optimized Al end cap to detector crystal distance is used for MCNP calculation. Thus, the radius of the detector crystal was systematically reduced; keeping the optimized Al end cap to crystal distance as 9 mm and efficiency ratios at two distances were obtained. Initially, when the radius was reduced by 0.8 mm, the efficiency ratio at the two distances, d = 1.7 and 21.7 cm, reduced to 1.03 and 1.01 respectively (Table 5.7). This indicates that the ratio is approaching 1 as desired.

Table 5.6 The comparison of experimental and MCNP efficiencies at two sample-to-detector distances, d = 1.7 cm and 21.7 cm. The MCNP efficiencies are computed by changing the Al end cap to detector crystal distance (d_{alc}) to see its effect on the detector efficiency.

Energy	**d_{alc} = 3 mm**	**d_{alc} = 6 mm**	**d_{alc} = 8 mm**	**d_{alc} = 8.5 mm**	**d_{alc} = 9 mm**	**d_{alc} = 10 mm**
(MeV)	**FEP efficiencies (MCNP/Exp)**					
	d = 1.7 cm					
0.088	1.53	1.32	1.21	1.18	1.15	1.10
0.122	1.49	1.28	1.17	1.14	1.11	1.07
0.136	1.49	1.29	1.17	1.14	1.12	1.07
0.279	1.36	1.18	1.08	1.06	1.03	0.99
0.320	1.44	1.25	1.14	1.11	1.09	1.04
0.661	1.41	1.22	1.12	1.10	1.07	1.03
1.115	1.50	1.30	1.19	1.16	1.14	1.09
Avg.	1.46	1.26	1.15	1.13	1.10	1.05
Std. Dev.	0.06	0.05	0.04	0.04	0.04	0.04
% RSD	3.92	3.86	3.77	3.76	3.78	3.71
	d = 21.7 cm					
0.088	1.14	1.11	1.09	1.08	1.08	1.07
0.122	1.16	1.13	1.11	1.11	1.10	1.10
0.136	1.14	1.12	1.10	1.09	1.09	1.07
0.279	1.13	1.11	1.09	1.09	1.08	1.07
0.320	1.11	1.08	1.06	1.05	1.05	1.04
0.661	1.17	1.15	1.13	1.13	1.12	1.13
1.115	1.15	1.12	1.10	1.10	1.10	1.09
Avg.	1.14	1.12	1.10	1.09	1.09	1.08
Std. Dev.	0.02	0.02	0.02	0.02	0.02	0.03
% RSD	1.90	2.02	2.02	2.03	2.02	2.48

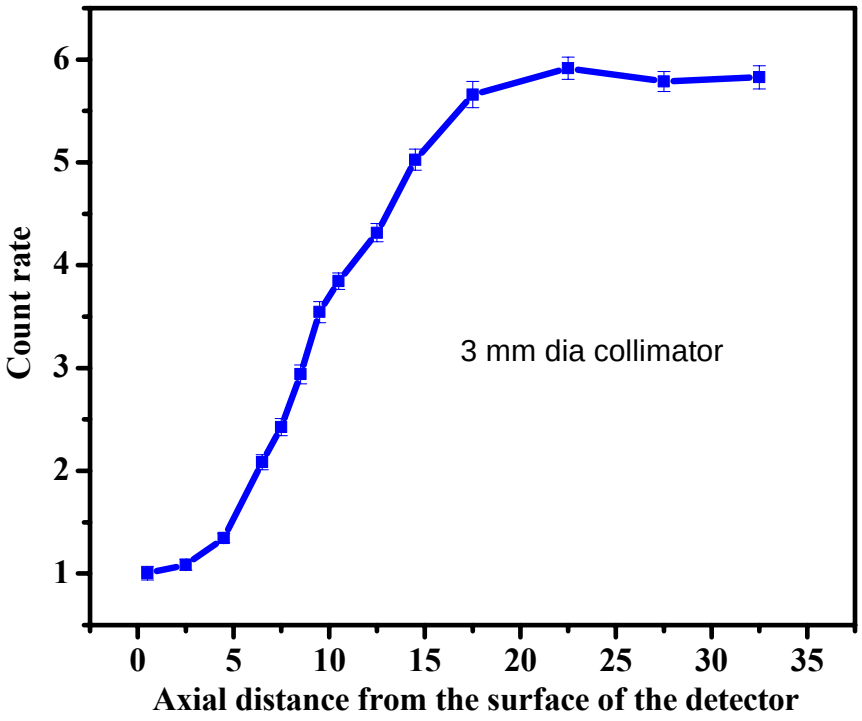

Figure 5.4 Axial profile of a collimated ^{109}Cd source from the surface of the detector.

Therefore, the radius was further reduced systematically in steps of 0.1 mm and the results are given in Table 5.7. When the radius is reduced by 0.9 mm, the average ratio at d = 1.7 cm and 21.7 cm was found to be close to unity, indicating that the manufacturer supplied crystal radius should be reduced by 0.9 mm to match the MCNP efficiencies with experimental efficiencies. But still at d = 1.7 cm, a slight systematic bias showing its dependence on energy was observed. The ratio of MCNP and experimental efficiencies was found to be higher at lower energies (1.10 at 88 keV) compared to higher energies (1.00 at 1115 keV). To remove this slight energy dependence, the dead layer thickness was increased by 0.1 mm. These calculations were done using the optimized Al end cap

to crystal distance and the optimized detector crystal radius. With this variation, the efficiency ratios were found to be within 5% at all energies and over all sample-to-detector distances. The experimental and the MCNP efficiencies calculated using this optimized geometry has been shown in Figure 5.5. The detector parameters for the optimized geometry have been given in the last column of Table 5.3.

Vargas et al. (2002) reported the effect of systematic variation of detector parameters on the simulated efficiencies of point and volumetric sources. The study showed that slight variation of detector parameters could lead to significant variation in detector efficiency. Of particular importance in the context of the present work, is the variation of efficiencies with the Al end cap to crystal distance for different source geometries. It has been observed [Vargas et al. (2002)] that this distance is critical for volumetric sources, but less important for point sources. However, our studies show that there is a strong distance dependence of simulated efficiencies with respect to experimental efficiencies for point sources also when manufacturer supplied detector parameters are used. It was also observed that this can be eliminated by adjusting the Al end cap to crystal distance.

Table 5.7 The comparison of experimental and MCNP efficiencies at two sample-to-detector distances, d = 1.7 cm and 21.7 cm. The MCNP efficiencies are computed by taking the optimized Al end cap to detector crystal distance as the basis and carrying out further optimization by changing the detector radius and dead layer thickness.

Energy (MeV)	**Al end cap to crystal distance, d_{alc} = 9 mm**			
	Nominal values of all other detector parameters	**Crystal radius reduced by 0.8 mm**	**Crystal radius reduced by 0.9 mm**	**Crystal radius reduced by 0.9 mm and dead layer increased by 1 mm**
	FEP efficiencies (MCNP/Exp)			
	d = 1.7 cm			
0.088	1.15	1.10	1.10	1.05
0.122	1.11	1.06	1.05	1.03
0.136	1.12	1.06	1.06	1.04
0.279	1.03	0.97	0.96	0.95
0.32	1.09	0.98	0.97	0.96
0.661	1.07	1.00	0.99	0.98
1.115	1.14	1.01	1.00	0.99
Avg.	1.10	1.03	1.02	1.00
Std. Dev.	0.04	0.05	0.05	0.04
% RSD	3.78	4.96	5.10	3.97
	d = 21.7 cm			
0.088	1.08	1.01	1.00	0.97
0.122	1.10	1.03	1.02	1.00
0.136	1.09	1.01	1.00	0.99
0.279	1.08	1.00	0.99	0.98
0.32	1.05	0.97	0.96	0.96
0.661	1.12	1.03	1.01	1.01
1.115	1.10	1.00	0.99	0.98
Avg.	1.09	1.01	1.00	0.98
Std. Dev.	0.02	0.02	0.02	0.02
% RSD	2.02	1.84	1.87	1.77

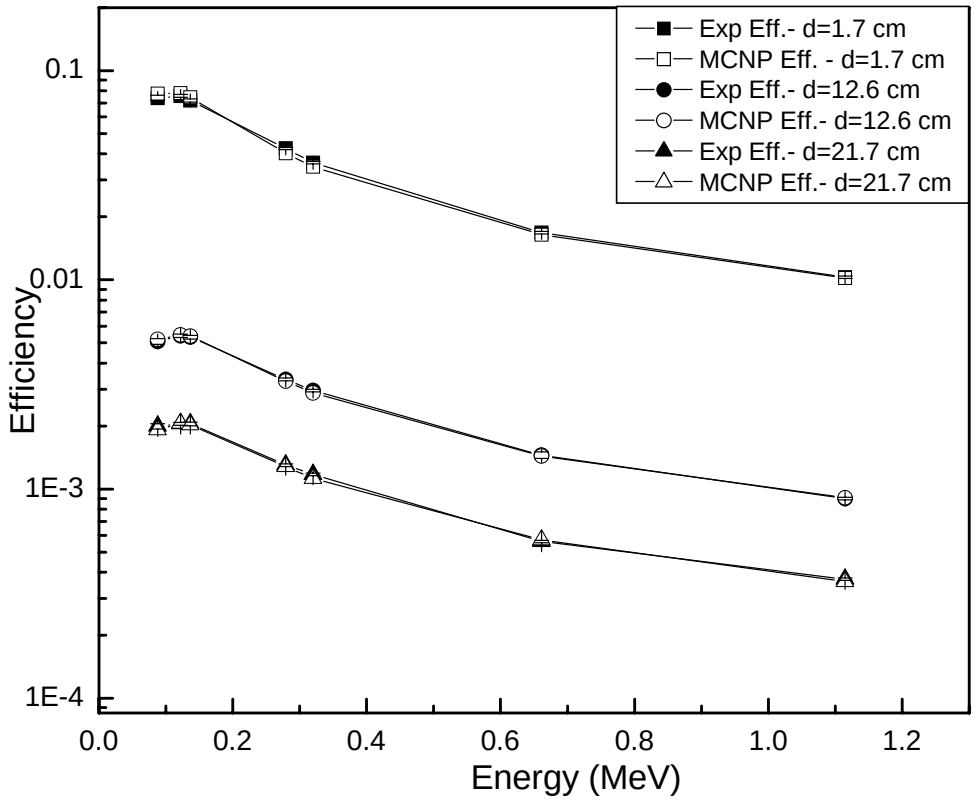

Figure 5.5 Experimental and MCNP simulated FEP efficiency for point source geometry using the optimized detector geometry at three sample-to-detector distances, d = 1.7 cm, 12.6 cm and 21.7 cm.

5.6 Efficiency Transfer to Volumetric Sources

In accordance with the principle of efficiency transfer, this optimized geometry should be valid for all the extended sample geometries. As a check of the optimized geometry, the efficiencies of 5 ml aqueous solutions of ^{109}Cd, ^{57}Co, ^{203}Hg, ^{137}Cs and ^{65}Zn in cylindrical vials at d = 2.0 and 10.3 cm were compared with the MCNP calculated efficiencies. The MCNP efficiencies for these samples were calculated using the optimized detector geometry and the detailed sample geometry. Table 5.8 gives the ratio of experimental and

MCNP efficiencies for 5 ml sources. The two efficiencies differ by about 7% at d = 2.0 cm and by 3% at d = 10.3 cm for this extended geometry.

Table 5.8 Ratios of MCNP to experimental efficiencies for 5 ml sources of ^{109}Cd, ^{57}Co, ^{203}Hg, ^{137}Cs and ^{65}Zn and for 100 ml ^{152}Eu source.

Energy	5 ml		**Energy**	100 ml
(MeV)	d=2.0 cm	d = 10.3 cm	**(MeV)**	d=19.8 cm
0.088	1.11	1.07	0.122	1.04
0.122	1.07	1.05	0.244	1.03
0.136	1.06	1.01	0.344	1.01
0.279	1.12	1.03	0.779	1.03
0.661	1.01	1.02	0.867	1.02
1.115	1.01	1.02	0.964	1.01
			1.112	1.04
			1.408	1.02
Avg.	1.07	1.03	**Avg.**	1.02
Std. Dev.	0.05	0.02	**Std. Dev.**	0.01
% RSD	4.46	2.06	**% RSD**	1.21

The validity of the optimized geometry was also checked for another extended source of standard 100 ml ^{152}Eu. The experimental efficiencies at d = 19.8 cm for this geometry were compared with the efficiencies calculated by using MCNP. The ratios of the two efficiencies are given in the last column of the Table 5.8. In this case also, the two efficiencies are within 3-4%. The slight difference in the efficiencies for volumetric samples at closer distance can be due to some inaccuracy in sample geometry such as its radius, glass thickness, its density and height. This has also been observed by Johnston et al. (2006) and Vargas et al. (2002) where it was concluded that the sample dimensions could have a significant effect on the detector efficiency. However our results of

simulated efficiencies using adjusted detector parameters based on point source efficiencies can be used for volumetric sources also and one can get results within 5%.

5.7 Conclusion

The MCNP can be used to get efficiencies for any sample geometry, once the detector geometry has been optimized to match the experimental and MCNP efficiencies. It is particularly useful when the standards are not available.